

# Tactile superresolution and biomimetic hyperacuity

Nathan F. Lepora, *Member, IEEE*, Uriel Martinez-Hernandez, *Student Member, IEEE*,  
Mathew Evans, Lorenzo Natale, Giorgio Metta and Tony J. Prescott

**Abstract**—Motivated by the impact of superresolution methods for imaging, we undertake a detailed and systematic analysis of localization acuity for a biomimetic fingertip and a flat region of tactile skin. We identify three key factors underlying superresolution that enable the perceptual acuity to surpass the sensor resolution: (i) the sensor is constructed with multiple overlapping, broad but sensitive receptive fields; (ii) the tactile perception method interpolates between receptors (taxels) to attain sub-taxel acuity; (iii) active perception ensures robustness to unknown initial contact location. All factors follow from active Bayesian perception applied to biomimetic tactile sensors with an elastomeric covering that spreads the contact over multiple taxels. In consequence, we attain extreme superresolution with a thirty-five fold improvement of localization acuity (0.12mm) over sensor resolution (4mm). We envisage that these principles will enable cheap, high-acuity tactile sensors that are highly customizable to suit their robotic use. Practical applications encompass any scenario where an end-effector must be placed accurately via the sense of touch.

**Index Terms**—Force and tactile sensing, biomimetics.

## I. INTRODUCTION

At present, the study of tactile superresolution in robotics is in its infancy. However, its potential to impact on tactile robotics is indicated by the advancements in technologies based on visual superresolution, which are revolutionizing the life sciences from cell biology to medical imaging ‘in ways unthinkable in the mid-90s’ [1], honored as a Nature ‘method of the year’ [2], and awarded the 2014 Nobel Prize in Chemistry (for superresolved fluorescence microscopy). In imaging, superresolution (SR) sensing encompasses a range of techniques for transcending the resolution limit (geometrical SR) and diffraction limit (optical SR) [3]. Artificial tactile sensors [4] tend to resemble their biological counterparts more closely than vision sensors (Sec. II-B) and diffraction effects are not relevant for tactile perception. Hence, the best methods for tactile superresolution will be distinct from those for visual superresolution, and may benefit greatly from adopting principles gained from the study of biological systems [5]. We thus consider tactile superresolution as biomimetic hyperacuity.

Manuscript submitted August 18, 2014; revised January 30, 2015 and March 9, 2015. This paper was recommended for publication by the Editor Brad Nelson upon evaluation of the reviewers comments. The work was supported in part by the European Commission under project WYSIWYD (ICT-612139) and by a University of Bristol pump priming award.

N. Lepora is with the Department of Engineering Mathematics, The University of Bristol, and the Bristol Robotics Laboratory (BRL), The University of Bristol and the University of the West of England (UWE), Bristol, UK. (email: n.lepora@bristol.ac.uk)

U. Martinez-Hernandez, M. Evans and T. Prescott are with the Sheffield Center for Robotics (SCentRo), University of Sheffield, UK. (email: mat.evans@shef.ac.uk, uriel.martinez@shef.ac.uk, t.j.prescott@shef.ac.uk).

L. Natale and G. Metta are with the Department of Robotics, Brain and Cognitive Sciences, Italian Institute of Technology (IIT), 16163 Genova, Italy (e-mail: lorenzo.natale@iit.it, giorgio.metta@iit.it).

Although biological hyperacuity is most widely studied in vision [6], it also occurs for touch and audition, and may be considered a general aspect of human and animal perception. For example, human touch can discriminate at  $\sim 0.3$  mm capacity [7], finer than the receptive fields of individual touch receptors ( $\sim 2$  mm [8]). No physical laws are broken because perception can involve spatial averages over the sensor distribution, which can transcend the resolution limit. Thus, nature has discovered design principles that allow perceptual systems to operate at finer acuity than might be expected from their sensory receptor densities and widths. These principles give lessons for robotics when optimizing sensor performance [5].

In this paper, we make a detailed and systematic analysis of localization superresolution for both a biomimetic fingertip with curved sensor morphology [9] and a planar region of tactile skin [10]. The computational framework in this paper is based on a general probabilistic approach for active tactile perception [11]–[14] that also relates to theories of perceptual decision making in biological systems. Here these methods are applied to localization of a single object (a cylinder) to examine the implications for tactile superresolution. Our study relies on a novel validation methodology that collects contact data at a very high spatial sampling density over each sensor’s entire location range. These data enable characterization of how localization acuity depends on the key factors underlying tactile perception, such as the receptive field properties from sensor construction and the resolution of the location classes. In particular, we find that active perception is key to obtaining a high degree of localization superresolution, because it can relocate the sensor to a region of fine acuity. In consequence, we obtain *extreme* tactile superresolution with a thirty-five fold improvement over sensor resolution.

These findings have implications both for the design of high acuity tactile sensors and the methods used for robot touch. A frequent assumption in tactile robotics is that ‘more taxels are better’ (or, equivalently, sensors with fewer taxels are criticized). However, we disagree. Perceptual acuity depends on a combination of factors, including taxel density, spatial layout, pressure sensitivity and receptive field size or shape [15], [16], coupled with utilizing active and probabilistic methods for perception [11]–[14]. Thus, to optimize sensor performance, constraints such as manufacturing costs and sensor robustness will necessitate a balance between these design factors, rather than focussing on any one in isolation. This balance will not necessarily involve having a high taxel density. For practical applications in future robotics, our expectation is that sensor optimization will be a sophisticated procedure, requiring modeling and empirical work to customize the design to suit a robot’s intended use.

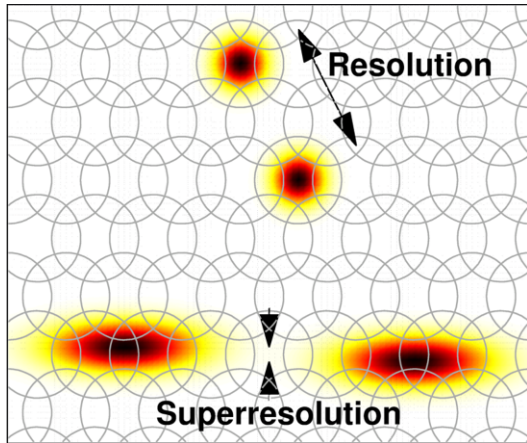


Fig. 1. Localization superresolution versus sensor resolution. Top: Two point-like (noisy) images on the receptor array can be resolved only if their separation leaves at least one intervening receptor with a detectably different intensity. Bottom: Two targets can be localized relative to each other to finer acuity than the receptor spacing; the superresolution mechanism achieves this by identifying the center of each target across all of the receptors it covers.

## II. BACKGROUND AND RELATED WORK

### A. Biological sensing and hyperacuity

Our senses, such as vision, audition and touch, take their inputs via sensory receptors that transduce stimuli from the physical world into signals appropriate for neural processing. For example, photoreceptors (vision) transduce light energy and mechanoreceptors (touch and audition) transduce kinetic energy into patterns of electrical spikes (*e.g.* [3], [4]). Each receptor has a receptive field, or region of space to which it responds, such as a cone of light rays onto a photoreceptor or a patch of skin activating a mechanoreceptor. For our senses to cover their nearby environment, receptors are packed together into overlapping arrays. The spacing between receptors then defines the sensor resolution, and relates to the minimum separation to distinguish two point-like stimuli (Fig. 1; top). For a healthy human eye, the angular resolution is about 1 arcmin (0.02 degs), or 30 cm at 1 km distance; for a human fingertip, the two-point discrimination is about 3 mm [7].

Acuity is the sharpness of perception, and depends on both the sensory apparatus and the computations underlying perception. Measures of acuity rely on quantifying the finest discriminable detail of a stimulus, such as the separation between two parallel lines (Vernier acuity). Computationally, perceptual acuity is aided by coarse coding mechanisms over multiple overlapping receptive fields, enabling parallel encoding of the stimulus appropriate for population averaging.

Hyperacuity is a perceptual effect where the acuity of perceiving stimulus detail is finer than the sensor resolution [6]. It has been studied primarily for human visual localization in situations where a spatially-extended stimulus activates many receptors, so that population averaged results have finer acuity than the sensor resolution (Fig. 1; bottom). Visual hyperacuity occurs for curvature detection, edge smoothness, stereoacuity (depth) and Vernier acuity. The highest hyperacuity measured with the human eye was the relative position of a line to 0.85 arcsec (0.0002 degs), equivalent to 4 mm at 1 km [17].

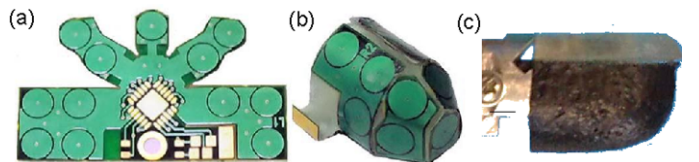


Fig. 2. Construction of tactile fingertip. A flexible PCB (a) is wrapped around a hard core (b) then covered in a soft silicon foam insulator and conductive rubber (c) to give a capacitive touch sensor. The lower plates of the 12 taxels are visible as circles on the PCB. (Figure adapted from [9].)



Fig. 3. Construction of planar region of tactile skin. A flexible PCB (a) is mounted on a solid base (b) then covered in a soft silicon foam insulator and (c) conductive fabric. (Figure adapted from [9].)

Human touch is also known to attain hyperacuity [7]: for static (~1 sec) touches against embossed spatial patterns, subjects estimated relative interval size to 0.3 mm and (modified Vernier) alignment to 0.4 mm. Both measurements are an order of magnitude better than the two-point discrimination interval (~3 mm) and the average spacing (~70/cm<sup>2</sup>) between (SA-I) mechanoreceptors in the fingertip. Practical benefits include Braille reading, which can involve sub-millimeter judgments of surface detail that depend upon tactile hyperacuity [7], [18].

### B. Artificial hyperacuity and robot tactile superresolution

Implementing localization hyperacuity with artificial sensors has been confined mainly to visual imaging, where it is known as *superresolution*, or more precisely *geometrical superresolution* [19]. Examples include sub-pixel localization [20] from interpolating over pixel distributions, and multi-exposure noise reduction [21] by averaging several images. One should be careful to distinguish these methods from *optical superresolution* [22], which is concerned with transcending the diffraction limit rather than the resolution limit [19]. Only geometrical superresolution is applicable to robot touch, because diffraction concerns the wave nature of light, which has no analogue in a contact-based sensory system. As mentioned in the introduction, we consider tactile superresolution as biomimetic hyperacuity, to emphasize that insights can be gained from biological sensing systems [5].

Standard geometrical SR techniques from image processing do not apply well to tactile robotics. Imaging techniques are based on hardware assumptions for conventional vision sensors which have planar two-dimensional arrays, minimal cross-talk between pixels and high pixel densities [19]. Conversely, most tactile sensors have complex geometries (*e.g.* Figs 3,4), significant cross-talk between tactile elements induced by the surface medium [16] and low tactile element densities. Moreover, tactile perception differs from computer vision in being innately active, in that all tactile measurements result from directly contacting an object, so that the nature of

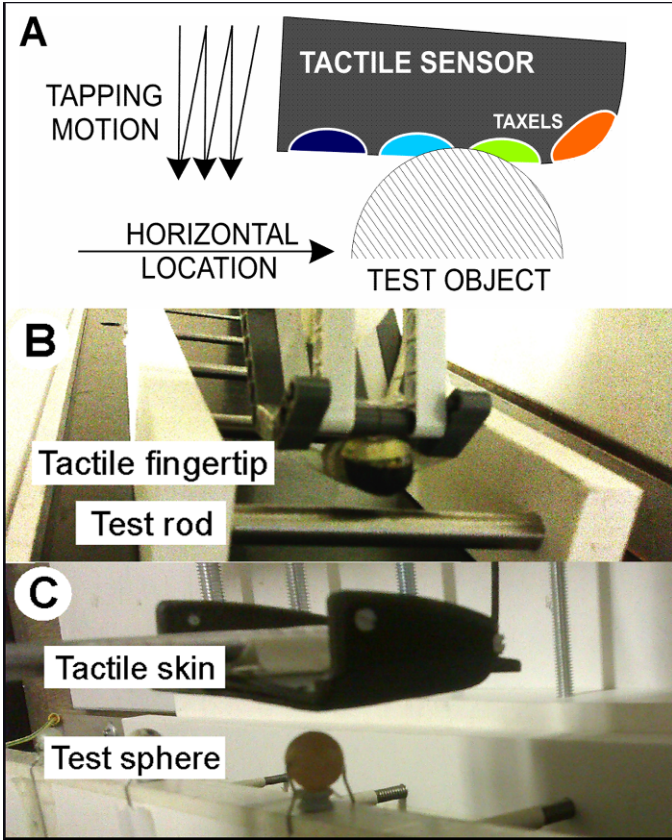


Fig. 4. Experimental setup. (A) Schematic of tactile sensor tapping against a cylindrical test object, with the pressure-sensitive taxels (colored) impinging onto the test object. For collecting training data, each tap is then followed by a small horizontal move to span the entire location range. (B) Forward view of the mounted fingertip tapping against a steel rod. (C) Side view of the planar tactile skin mounted on the Cartesian robot tapping against a rod. These experimental setups are ideal for systematic data collection to characterize the properties of the sensor interacting with objects.

the physical contact and how the robot is controlled during perception cannot be ignored.

Biomimetic hyperacuity is particularly relevant for robot touch because tactile sensors are often designed to resemble their biological counterparts in important aspects, which is less the case with vision sensors. Because tactile sensors function by contact mediated through a surface skin, the cross-talk between neighboring tactile elements (taxels) [16] is analogous to the overlap between neighboring sensory receptors in biological systems. Moreover, tactile sensors can have resolution of order one millimeter and broad receptive fields, similar to a human fingertip (for example, the sensors in this study); however, it is not yet possible to construct vision sensors with receptive field properties like those of the human eye. These aspects of robot touch and more suggest that the human sense of touch gives a firm foundation on which to base the tactile capabilities of robots [4].

Few studies have considered hyperacuity or superresolution sensing in robot touch. The only study considering tactile hyperacuity from a biomimetic perspective demonstrated a localization acuity finer than the (4 mm) taxel spacing [11]. However, the methods suffered (in hindsight) from being somewhat *ad hoc* and the tactile dataset was taken over an

incomplete location range with a low sampling density that limited the attained acuity to poorer than 1 mm. A superior treatment [13] focussing on active perception also exhibited hyperacuity but again used data with low spatial sampling density, and was also not a dedicated study of hyperacuity. Another previous study used digital image processing techniques for multi-exposure noise reduction [23], and also found the importance of actively controlling the contact, similarly to the other studies of tactile hyperacuity. However, the image processing methods relied on having flat tactile arrays, whereas fingertip-based sensors such as the one considered here are curved. Moreover, tactile data is commonly from dynamic contacts, such as taps, whereas imaging techniques rely on single images (or many versions of the same image). Potential benefits of superresolution sensing for robot touch have also been noted, both by reducing the complexity of sensor construction with fewer tactile elements and in easing up the processing requirements of the tactile system [15], [16].

### III. MATERIALS AND METHODS

#### A. Tactile robots and experiments

Two tactile sensor variants are used in this study (Figs 2,3) that were designed as a tactile fingertip [9] and planar skin [10]. The tactile fingertip has a rounded morphology of dimensions 14.5 mm long by 13 mm wide (Fig. 2A), covered with  $N_{\text{taxels}} = 12$  pressure sensitive taxels. The tactile skin has 4 equilateral triangular-shaped taxel arrays in a planar layout, each 30 mm wide and covered with 12 taxels (Fig. 2B); of these we used 3 arrays along the bottom of the sensor with  $N_{\text{taxels}} = 36$ . These tactile sensors detect pressure by the capacitance change due to a compressible insulating layer between the inner conducting plate of the taxels and an electrically conductive outside layer. The two sensors have a similar construction for the inner conducting plates (a flexible PCB) and insulating layer (soft silicone foam, 2 mm deep), but differ in their outside layer: the fingertip uses conductive silicone rubber, whereas the skin uses conductive Lycra-like fabric. For more details of their construction, we refer to the original reference on the technologies for the implementation of large-scale robot tactile sensors [9], [10].

Here we mount each tactile sensor as an end effector on a two degree-of-freedom Cartesian robot (2-axis PXYx, Yamaha Robotics). This combination of tactile sensor with Cartesian robot has been employed previously for testing various tactile sensors, including tactile vibrissae [24], [25] and tactile fingertips [11]–[14], [26]. The Cartesian robot has the benefit that it can precisely and repeatedly position the sensor in two dimensions (absolute repeatability 0.02 mm). As such, it is an ideal platform to probe tactile sensing; for example, by tapping the sensor against various test objects over a systematic and exhaustive range of locations.

The present study focusses on the tangential localization acuity of a curved object impinging against the tactile sensor surface. Both variants of tactile sensor were mounted with their (horizontal) sensing surface oriented perpendicular to the (vertical) direction of the tapping motion (Fig. 4A). For both sensors, a smooth steel cylindrical rod (diameter

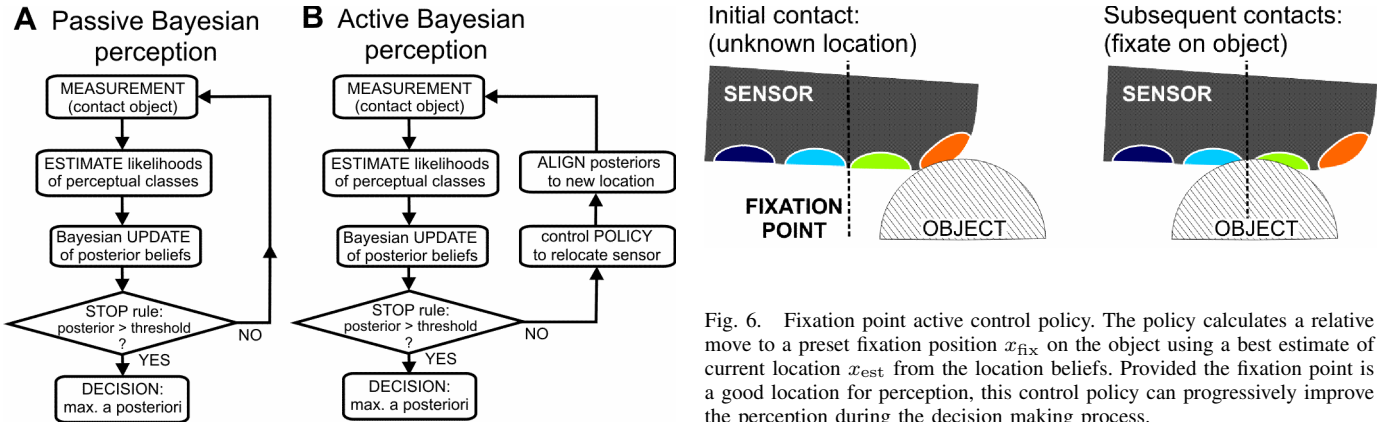


Fig. 5. Passive and active Bayesian perception. (A) Passive Bayesian perception has a recursive belief update with decision termination when the posterior belief reaches threshold. (B) Active Bayesian perception has the same recursive belief update, while also controlling sensor location according to a belief-based control policy. Upon moving the sensor, the location components of the posterior beliefs are re-aligned with the new sensor location. The two algorithms differ only in the control loop for active Bayesian perception.

6.4 mm=3/8 in.) was used as a test object (fingertip: Fig. 4B; skin: Fig. 4C). The perceptual task was to determine the tangential (horizontal) location of the test object by tapping against it.

Touch data were collected while the tactile sensor tapped down onto the test object followed by a diagonal move back up to a height 20 mm above the surface with a horizontal displacement  $\Delta x$ , before making the next tap (Fig. 4A). The displacement  $\Delta x = 0.01$  mm was near the accuracy limit of the Cartesian robot, with results taken over spans of 10 or more taps, collectively above this limit. For the curved fingertip, a horizontal  $x$ -range of 30 mm was used, giving 3000 taps across the cylindrical object. For the planar skin, a horizontal  $x$ -range of 60 mm was used, giving 6000 taps across the rod. From each tap of a tactile sensor against the test object, a 1 sec time series of pressure readings ( $N_{\text{samples}} = 50$ ) was extracted for all  $N_{\text{taxels}}$  taxels. A 1 sec pause was taken between brief ( $\sim 0.1$  sec) contacts to ensure transients decayed; no noticeable hysteresis then occurred, as seen directly from Figs 9,12.

The data used later in this paper were collected twice to give distinct training and test sets. This approach for validation ensured that the results are based on sampling from an independent data set to that used to train the classifier, with differences between the sets being characteristic of the accuracy and repeatability of the robot and the noise of the sensor reading (both from variations in the contact and intrinsic sensor noise). The variability between data sets was similar to that of adjacent taps within each set, with coefficient of variation 0.2 in the center of the range decreasing to 1 at the extremities (envelope similar to Fig. 12A). Data were collected at 8 bit resolution (peak response 256) and then high-pass filtered [9]. Pressure scales for the tactile fingertip and skin sensors are given in ref. [27].

### B. Bayesian perception for robotics

We use a Bayesian perception method for classifying object location that is based on sequential analysis models of percep-

Fig. 6. Fixation point active control policy. The policy calculates a relative move to a preset fixation position  $x_{\text{fix}}$  on the object using a best estimate of current location  $x_{\text{est}}$  from the location beliefs. Provided the fixation point is a good location for perception, this control policy can progressively improve the perception during the decision making process.

tual decision making in neuroscience and psychology [28], [29]. Sequential analysis is a statistical technique for hypothesis selection over data that is sequentially sampled until reaching a stopping condition [30], which commonly takes the form of a threshold on the posterior belief. Its application to neuroscience and psychology rests on the empirical success in modeling behavioral experiments (e.g. reaction time distributions) and also that neuronal activity during decision making is consistent with a threshold crossing. Theoretically, hypothesis selection via a decision threshold is known to optimize decision making under some circumstances (e.g. two choices with a linear cost function of decision time and error rate).

This Bayesian perception approach has been applied successfully to robot tactile perception [11]–[14], [26], [31], [32]. The method implements a recursive Bayesian update of the posterior beliefs for each distinct perceptual class (the statistical hypotheses) until reaching a predefined decision threshold. Here we consider two implementations of Bayesian perception (Fig. 5), termed active and passive, depending on whether or not the sensor can relocate during perception. Although we here apply these methods to purely localization decisions, they have more general applicability [13].

Passive Bayesian perception accumulates belief for  $N_{\text{loc}}$  distinct location classes  $x_l$  by making successive taps  $z_t$  against a test object until at least one of the posterior location beliefs  $P(x_l|z_{1:t})$  crosses a decision threshold  $\theta_{\text{dec}}$ , when the localization decision  $x_{\text{dec}}$  is made. The passive nature of the perception means that the location class  $x_l$  is constant over the decision making process (Fig. 5A).

Active Bayesian perception also accumulates belief for the location classes  $x_l$  by successively tapping until a posterior belief  $P(x_l|z_{1:t})$  reaches a predefined decision threshold  $\theta_{\text{dec}}$ , but in addition utilizes a posterior-dependent control policy  $\pi$  to move the sensor during the perceptual process (Fig. 5B). This control policy takes as input the posterior beliefs and outputs a relative move to a new location class. In accordance, the posteriors must be re-aligned with the new location class, by shifting the class index by the number of classes moved. Active perception encompasses any non-trivial control policy, although the speed and quality of perception will depend on the policy and the perceptual task performed.

Here we focus on a ‘fixation point’ control policy inspired

**Algorithm** Active Bayesian perception

---

```

for l=1 to  $N_{\text{loc}}$  do
    Sample  $z = \{s_k(j)\}$  from location  $x_l$ 
    Pre-compute  $P(b|k, l)$  histograms (bins  $b_k(j)$  of  $s$ )
end for
 $t = 0$ 
Initialize  $x$ ; e.g.  $x = \text{rand}(1 \cdots N_{\text{loc}})$ 
Define policy; e.g.  $\pi(x) = x - x_{\text{fix}}$ 
 $P(x_l|z_0) = 1/N_{\text{loc}}$ 
while  $\max_l P(x_l|z_{1:t}) < \theta_{\text{dec}}$  do
     $t \leftarrow t + 1$ 
    Sample  $z_t = \{s_k(j)\}$  from current location  $x$ 
    for l=1 to  $N_{\text{loc}}$  do
         $\log P(z_t|x_l) = \sum_{k=1}^{N_{\text{taxels}}} \sum_{j=1}^{N_{\text{samples}}} \frac{\log P(b_k(j)|k, l)}{N_{\text{samples}}N_{\text{taxels}}}$ 
         $P(x_l|z_{1:t}) = P(z_t|x_l)P(x_l|z_{1:t-1})/P(z_t|z_{1:t-1})$ 
    end for
     $x_{\text{est}}(t) = \arg \max_{x_l} P(x_l|z_{1:t})$ 
     $x \leftarrow x + \pi(x_{\text{est}})$ 
     $P(x_l|z_{1:t}) \leftarrow P(x_l - \pi(x_{\text{est}})|z_{1:t})$  (with correction)
end while
 $x_{\text{loc}} = \arg \max_{x_l} P(x_l|z_{1:t})$ 

```

---

by human and animal vision, where the fovea is fixated onto an object to best perceive its location or identity (e.g. [33], [34]). The sensor is actively controlled during perception to attain a preset location class  $x_{\text{fix}}$  on the object, by making a relative move after each tap given by the difference of the current estimated location and fixation point (Fig. 6). The performance depends on having a good fixation point: in this study, we simply use the center of the location range, which was aligned with the object (although not considered here, it is also possible to learn the fixation point [26]). Then the control policy progressively improves the perception during the decision process from an initially unknown location (Fig. 7B).

Formally, the Bayesian perception method applies to sequences of contact data  $z_{1:t} = \{z_1, \dots, z_t\}$ , each of which is a multi-dimensional time series of sensor values,

$$z_t = \{s_k(j) : 1 \leq j \leq N_{\text{samples}}, 1 \leq k \leq N_{\text{taxels}}\}, \quad (1)$$

with indices  $j, k$  labeling the time samples and sensor taxels respectively. This contact data gives evidence for the present location class  $x_l$ ,  $1 \leq l \leq N_{\text{loc}}$ , computed through the algorithms in Fig. 5, with details as follows.

*1) Measurement model and likelihood estimation:* The location likelihoods  $P(x_l|z_t)$  are found using a measurement model of the contact data, based on a non-parametric method applied to sampling distributions from training data over the

distinct location classes [31], [35]. First, sensor values  $s_k$  for taxel  $k$  are binned into equal intervals  $I_b$ ,  $1 \leq b \leq N_{\text{bins}}$ , with sampling distribution given by the normalized histogram  $h(b, k, l)$  over all training data for each location class  $x_l$ :

$$P(b|k, l) = \frac{h(b, k, l)}{\sum_{b=1}^{N_{\text{bins}}} h(b, k, l)}, \quad (2)$$

where  $h(b, k, l)$  is the sample count in bin  $b$  for taxel  $k$  over all training data in class  $x_l$ . Then, given a test contact  $z_t$  with samples  $s_k(j)$ , we construct a measurement model from the mean log likelihood over all samples in that contact

$$\log P(z_t|x_l) = \sum_{k=1}^{N_{\text{taxels}}} \sum_{j=1}^{N_{\text{samples}}} \frac{\log P(b_k(j)|k, l)}{N_{\text{samples}}N_{\text{taxels}}}, \quad (3)$$

where  $b_k(j)$  is the bin occupied by sample  $s_k(j)$ . Technically, this measurement model becomes ill-defined if any histogram bin is empty, which is easily fixed by regularizing the bin counts with a small constant ( $\epsilon \ll 1$ ), giving  $h(b, k, l) + \epsilon$ .

*2) Bayesian belief update:* Bayes' rule is used after each successive test contact  $z_t$  to recursively update the posterior location beliefs  $P(x_l|z_{1:t})$  for the perceptual classes with the location likelihoods  $P(z_t|x_l)$  of that contact data

$$P(x_l|z_{1:t}) = \frac{P(z_t|x_l)P(x_l|z_{1:t-1})}{P(z_t|z_{1:t-1})}, \quad (4)$$

from background information given by the prior location beliefs  $P(x_l|z_{1:t-1})$  (i.e. the posterior beliefs from the preceding contact). The marginal probabilities  $P(z_t|z_{1:t-1})$  of the current contact given the prior contact history are also conditioned on the preceding contacts  $z_{1:t-1}$  and given by

$$P(z_t|z_{1:t-1}) = \sum_{l=1}^{N_{\text{loc}}} P(z_t|x_l)P(x_l|z_{1:t-1}). \quad (5)$$

Iterating (4,5), a sequence of contacts  $z_1, \dots, z_t$  results in a sequence of posterior beliefs  $P(x_l|z_1), \dots, P(x_l|z_{1:t})$  initialized from uniform prior beliefs  $P(x_l|z_0) := P(x_l) = 1/N_{\text{loc}}$ .

*3) Final location decision:* For passive perception, we follow sequential analysis methods for optimal decision making that recursively update beliefs up to a threshold  $\theta_{\text{dec}}$  that triggers the final decision (Fig. 8A). Thus, the update (4,5) stops when the posterior location belief  $P(x_l|z_{1:t})$  passes a threshold  $\theta_{\text{dec}}$ , giving a final location decision  $x_{\text{dec}}$  from the maximal *a posteriori* (MAP) estimate at time  $t_{\text{dec}}$

$$\text{if any } P(x_l|z_{1:t}) > \theta_{\text{dec}} \text{ then } x_{\text{dec}} = \arg \max_{x_l} P(x_l|z_{1:t}). \quad (6)$$

$b$	bin index	$N_{\text{bins}}$	number of bins	$s$	sensor value	$z_{1:t}$	contact history to time $t$
$e_{\text{loc}}$	location error	$N_{\text{loc}}$	number of locations	$t$	time index	$z_t$	contact at time $t$
$h(b, k, l)$	sample histogram	$N_{\text{samples}}$	number of samples	$t_{\text{dec}}$	decision time	$\pi$	movement policy
$I_b$	bin interval	$N_{\text{taxels}}$	number of taxels	$x_l$	location class	$\theta_{\text{dec}}$	decision threshold
$j$	sample index	$P(x_l z_{1:t})$	location belief	$x_{\text{est}}$	estimated location		
$k$	taxel index	$P(z_t x_l)$	location likelihood	$x_{\text{dec}}$	decided location		
$l$	location index	$P(z_t z_{1:t})$	marginal probability	$x_{\text{fix}}$	fixation location		

TABLE I  
SYMBOLS GLOSSARY.

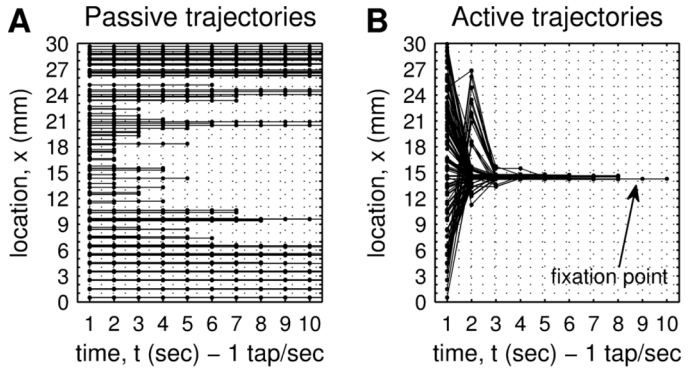


Fig. 7. Example trajectories for passive and active perception. 100 trajectories were selected randomly for each case (decision threshold  $\theta_{dec} = 0.95$ ). (A) Passive perception, with sensor location  $x$  constant over time. (B) Active perception, with trajectories  $x(t)$  converging on the central fixation point  $x_{fix}$  independent of starting position.

This decision threshold  $\theta_{dec}$  is a free parameter that adjusts the balance between decision time  $t_{dec}$  and accuracy  $e_{loc}$ . For a choice between two outcomes this speed-accuracy balance can be proved optimal [30]; optimality is not known for the many perceptual choices considered here, so we make a reasonable assumption of near optimality [31].

4) *Active perception of location:* Our method for active perception is based on the above passive method, with the addition of a posterior-dependent control policy  $\pi$  to move the sensor during the perceptual process. This policy takes as input the posterior beliefs (or a quantity derived from them) and outputs a relative move to a new location.

Here we consider an active control policy  $\pi$  for moving the sensor  $x \leftarrow x + \pi(x_{est})$  that depends only on an intermediate estimate of object location

$$x_{est} = \arg \max_{x_l} P(x_l | z_{1:t}). \quad (7)$$

Upon performing the resulting move, the location beliefs  $P(x_l | z_{1:t})$  should be kept aligned with the sensor by shifting them by the number of classes moved

$$\begin{aligned} & \text{if } 1 \leq x_l - \pi(x_{est}) \leq N_{loc} \text{ then} \\ & \quad P(x_l | z_{1:t}) \leftarrow P(x_l - \pi(x_{est}) | z_{1:t}), \\ & \text{if } x_l - \pi(x_{est}) < 1 \text{ or } x_l - \pi(x_{est}) > N_{loc} \text{ then} \\ & \quad P(x_l | z_{1:t}) \leftarrow p_0, \end{aligned} \quad (8)$$

where we recalculate the beliefs  $p_0$  lying outside the original range by assuming they are uniformly distributed and the shifted beliefs  $P(x_l | z_{1:t})$  sum to unity. The left arrow denotes that the quantity on the left is replaced with that on the right.

For simplicity, here we consider a ‘fixation point’ policy [12], [13] motivated by orienting movements in animals: the control policy attempts to move the sensor to a predefined fixation point  $x_{fix}$  relative to the object assuming it is at the estimated location  $x_{est}$  on the object,

$$x \leftarrow x + \pi(x_{est}), \quad \pi(x_{est}) = x_{fix} - x_{est}, \quad (9)$$

where  $x$  is the actual (unknown) location of the sensor. In practice, only the move  $\pi(x_{est})$  need be found, to instruct the sensor how to change relative location. Provided the fixation

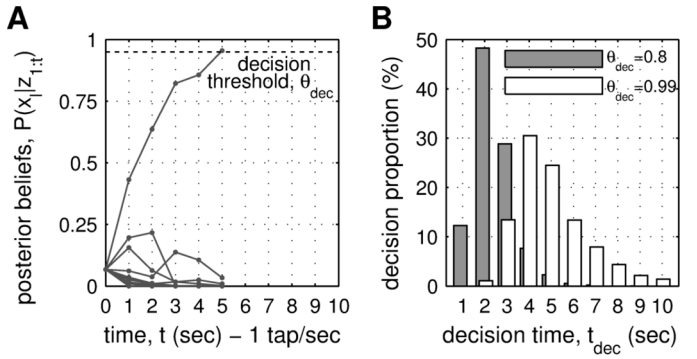


Fig. 8. Effect of decision threshold on perception. (A) Example decision, with evidence integrated over successive taps until a location belief  $P(x_l | z_{1:t})$  crosses the decision threshold  $\theta_{dec}$ . Each curve corresponds to the probability for a different location class  $x_l$ . (B) Histograms of decision times  $t_{dec}$  across many decisions; the distribution peak shifts to longer times for increased decision thresholds.

point is set to be a good location for perception, this control policy will progressively improve the perception during the decision making process from an initially unknown location where the perception may be poor. Here we will assume the fixation point to be at the center of the location range, although this is a quantity that can itself be optimized [26].

### C. Virtual environment estimate of location acuity

The aim of our data collection is to set up a ‘virtual environment’ in which methods for perception can be compared off-line on identical data. This is achieved by measuring contact signals over an exhaustive range of object locations. We can then use Monte Carlo validation to ensure good statistics: perceptual errors are averaged over many test runs with contact data drawn randomly from the perceptual classes (typically 10000 runs per data point plotted in the results).

For analysis, the data were separated into  $N_{loc}$  distinct classes, by collecting groups of contact data each spanning part of the overall range. For the tactile fingertip, we considered 10, 15, 30, 60, 100, 150, 300 location classes spanning a 30 mm range (class widths 3, 2, 1, 0.5, 0.3, 0.2, 0.1 mm). For the tactile skin, we considered 30, 60, 120, 240, 300, 600 location classes spanning a 60 mm range (class widths 2, 1, 0.5, 0.25, 0.2, 0.1 mm).

The localization error  $e_{loc}(x)$  is quantified with the mean absolute error  $|x - x_{dec}|$  over all classified  $x_{dec}$  location values for all test runs with true location class  $x$ . Then the mean localization error  $\bar{e}_{loc} = \sum_{l=1}^{N_{loc}} e_{loc}(x_l) / N_{loc}$  is averaged over all location classes  $x_l$ . The decision time  $t_{dec}(x)$  and mean decision time  $\bar{t}_{dec}$  are defined similarly.

Perceptual acuity can then be defined as the maximum of the mean localization error  $\bar{e}_{loc}$  and the class width. For large class widths (small  $N_{loc}$ ), the mean error is less than the class width, so the class width limits the perception; for small classes (large  $N_{loc}$ ), the error is larger than the class width, and the localization error limits the perception.

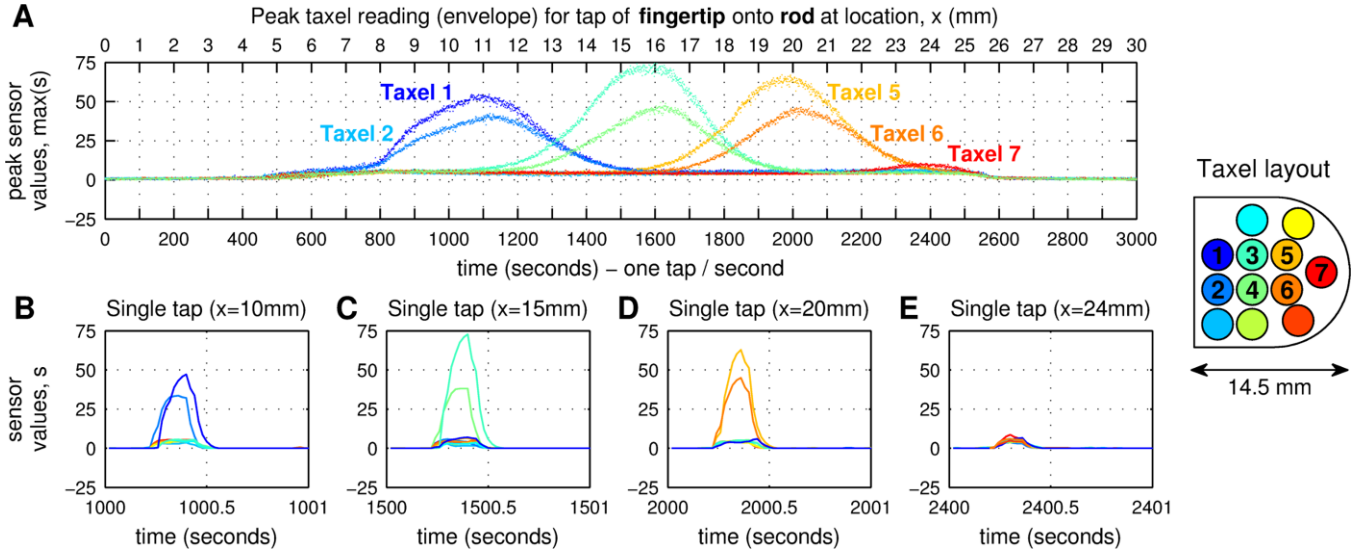


Fig. 9. Tactile data for fingertip relative to rod. Contacts at constant rate of 1 tap/second with 0.01 mm displacement after every tap to span a 30 mm location range with 3000 taps. (A) Envelope taken from peak taxel readings. (B-E) Examples of individual taps. Taxels are colored by their layout on the fingertip. Sensor responses are collected at 8-bit resolution (maximum value 256); comparison with a pressure scale is given in ref. [27, Fig. 9].

#### IV. RESULTS

##### A. Tactile fingertip

1) *Inspection of data:* Data for the tactile fingertip (Fig. 9) were collected while the sensor tapped repeatedly up and down against the test object (cylindrical rod, 6.4 mm diameter) with a small horizontal displacement after each tap to sample across a 30 mm location range. The initial and final parts of the data collection are for contacts either at the fingertip's non-sensitive base or missing the object entirely, with little or no tactile response. Between these extremes, the first sensed contacts are with the taxels at the sensor's base, followed by the middle taxels and finally the taxels at its curved tip. Each taxel has a broad, Gaussian-shaped receptive field about 8 mm across with centers spaced about every 4 mm (Fig. 9A). Individual taps typically take  $\sim 0.1$  sec to reach peak amplitude, followed by a rapid decay to baseline (Figs 9B-E). Hence, contact features from the stimulus are encoded both in the time-series response of each taxel and in which taxels are activated.

The most obvious effect of varying horizontal contact location of the fingertip against the object was a change in taxel identity and peak response amplitude. For each contact, the pattern of taxel pressures depends on the location of the fingertip relative to the object, permitting classification of where the rod is located relative to the fingertip. The geometry of the overlapping receptive fields implies that multiple taxels are activated simultaneously, so that the contacted stimuli are coarse-coded over multiple sensor outputs. We will see that

these aspects of the data are important for the perceptual acuity of localizing the object being sensed.

2) *Passive Bayesian perception:* The perceptual acuity of the fingertip for locating the rod is assessed first with a passive Bayesian method for robot perception. Bayesian perception updates the posterior beliefs  $P(x_l|z_{1:t})$  for  $N_{\text{loc}}$  distinct location classes  $x_l$ , using successive taps  $z_1, \dots, z_t$  against a test object until at least one belief crosses a decision threshold  $\theta_{\text{dec}}$ . Results are generated with a Monte Carlo procedure using the data as a virtual environment (Sec. III-C), such that each contact tap *passively* remains at its initial location class (example trajectories in Fig. 8A).

Passive perceptual decisions of object location are evaluated for decision thresholds  $\theta_{\text{dec}}$  from 0-0.999, over  $N_{\text{loc}} = 30$  location classes spanning the 30 mm range across the fingertip (Fig. 10). Perceptual error depends strongly on test location class, with mean localization error  $e_{\text{loc}}(x)$  increasing sharply at the extremes of the horizontal range from small errors in the central region (Fig. 10A). The lowest errors  $e_{\text{loc}}(x) \lesssim 0.2$  mm are in the region nearby the mid-point  $x = 15$  mm of the 30 mm range. Decision times  $t_{\text{dec}}(x)$  are modified from a U-shaped function (Fig. 10B), by also having a central spike that coincides with the maximum of the middle taxel's receptive field (similar spikes also occur for adjacent taxels at 10 mm and 20 mm). Our interpretation of this effect is that tactile acuity can be improved by contacts with multiple taxel receptive fields (*e.g.* near 13 mm and 18 mm); meanwhile, the overall U-

number of classes, $N_{\text{loc}}$	10	15	30	60	100	150	300
class width, $x_{\text{class}}$	3 mm	2 mm	1 mm	0.5 mm	0.3 mm	0.2 mm	0.1 mm
mean decision error, $\bar{e}_{\text{loc}}$ (passive perception)	4.6 mm	4.5 mm	4.4 mm	4.4 mm	4.5 mm	4.6 mm	4.5 mm
mean decision error, $\bar{e}_{\text{loc}}$ (active perception)	0 mm	0 mm	0.01 mm	0.04 mm	0.07 mm	0.08 mm	0.12 mm
acuity, $\max(x_{\text{class}}, \bar{e}_{\text{loc}})$ (active perception)	3 mm	2 mm	1 mm	0.5 mm	0.3 mm	0.2 mm	0.12 mm

TABLE II

ACTIVE PERCEPTUAL ACUITY DEPENDS ON LOCATION CLASS WIDTH. RESULTS ARE FOR MEAN DECISION TIMES OF 2 TAPS.

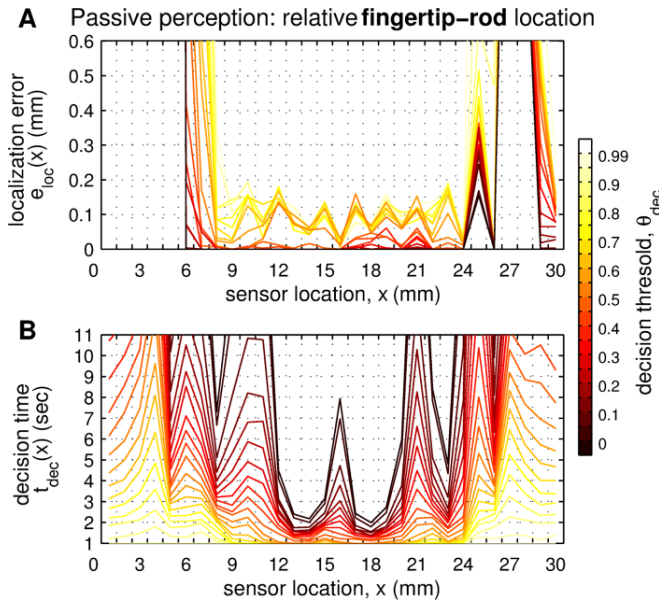


Fig. 10. Acuity of passive Bayesian perception depends on relative fingertip-rod location and decision threshold. (A) Localization errors  $e_{loc}(x)$  and (B) decision times  $t_{dec}(x)$  plotted against sensor location class  $x_l$ , with the color-scale denoting decision threshold  $\theta_{dec}$  (10000 trials per threshold, with  $N_{loc}=30$  location classes). Perceptual performance is best in the central region of the location range and for higher decision thresholds.

shaped function of accuracy is consistent with contacts at the extremities contacting fewer taxels and becoming being weak on the edge of their receptive fields and on the curved tip.

For passive perception, there is no control over the location from where an object is sensed. Hence, we typify the location accuracy for the fingertip and rod as a mean localization error  $\bar{e}_{loc}$  over all possible sensing locations (Fig. 11A, red plot). Given  $\bar{e}_{loc} \sim 4.5$  mm, this gives a poor location acuity dominated by the poor perception on the extremities of the range. These results emphasize that passive perception performs poorly because it cannot control contact location.

3) *Active Bayesian perception:* Next, we assess the perceptual acuity of the fingertip locating a rod with an active method for robot perception. Active Bayesian perception accumulates location belief  $P(x_l|z_{1:t})$  up to a decision threshold  $\theta_{dec}$ , as in passive perception; however, in addition, a control policy attempts to relocate the sensor between taps according to these location beliefs. Here we use a ‘fixation point’ policy, in which a best estimate of current location is used to calculate a relative move to a fixed location on the object (example trajectories in Fig. 7B). We take this fixation point in the center of the fingertip’s location range ( $x_{fix} = 15$  mm), where the passive perception had good acuity. The range of decision thresholds  $\theta_{dec} = 0\text{-}0.999$  remains unchanged from the previous section, to permit comparison of the active and passive approaches.

Active perceptual decisions of object location are again started from random locations, so we measure performance by the mean localization error  $\bar{e}_{loc}$  over all initial contact locations (Fig. 11; green plots). The best accuracies were for the higher decision thresholds (Fig. 11A) corresponding to mean decision times  $\bar{t}_{dec}$  greater than two taps (Fig. 11C). Even for two taps, the active perception reaches a mean error  $\bar{e}_{loc} \lesssim 0.12$  mm, an

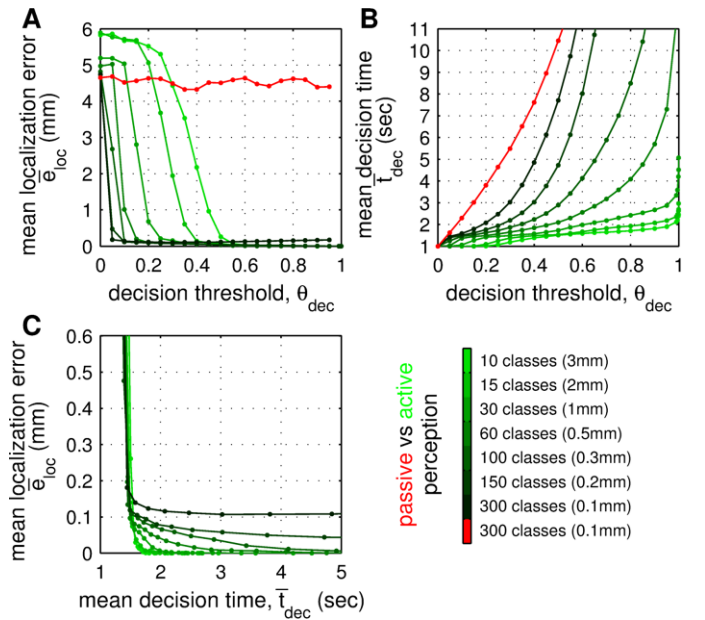


Fig. 11. Location-averaged performance for active and passive perception with the fingertip. (A) Mean localization errors  $\bar{e}_{loc}$  and (B) decision times  $\bar{t}_{dec}$  plotted against decision threshold (10000 trials per threshold). Passive perception is shown in red and active perception in green, shaded by location class number  $N_{loc}$ . (C) Mean localization error plotted against mean decision time (with threshold an implicit parameter). Active performs better than passive perception, and both improve with increasing decision threshold and decreasing class number.

order of magnitude better than passive perception ( $\sim 4.5$  mm) and the (4 mm) spacing between taxels (Table II).

Perceptual performance also depends on the number of location classes, considered over  $N_{loc} = 10\text{-}300$  with location class resolution  $30/N_{loc}$  mm. Thus, both the mean localization error  $\bar{e}_{loc}$  and mean decision time  $\bar{t}_{dec}$  depend on the class number  $N_{loc}$  and decision threshold  $\theta_{dec}$ , with their variation with threshold more rapid for larger class numbers (Figs 11A,B). This variability partially cancels in the speed-accuracy curves of mean localization error against mean decision time (Fig. 11C) until the error falls to an asymptote. The best location error then depends on class number, with mean errors increasing from  $\bar{e}_{loc} = 0.00$  mm (10 classes) to 0.12 mm (300 classes), while class resolution decreases from 3 mm to 0.1 mm (Table II). Thus, localization acuity and class resolution become similar for 300 classes, giving a best perceptual acuity of 0.12 mm.

Considering the taxel spacing is 4 mm for the fingertip, active perception gave a localization superresolution with thirty-five fold improvement over sensor resolution.

### B. Planar tactile skin

1) *Inspection of raw data:* Data for the tactile skin (Fig. 9) were collected while the sensor tapped repeatedly up and down against the test object (cylindrical rod 6.4 mm diameter) with a small horizontal displacement after each tap to sample across a 60 mm location range. At the beginning of the data collection only the taxels on the left of the skin are in contact, then the middle taxels and finally the taxels at the right. Each taxel has a broad, Gaussian-shaped receptive field about 16 mm

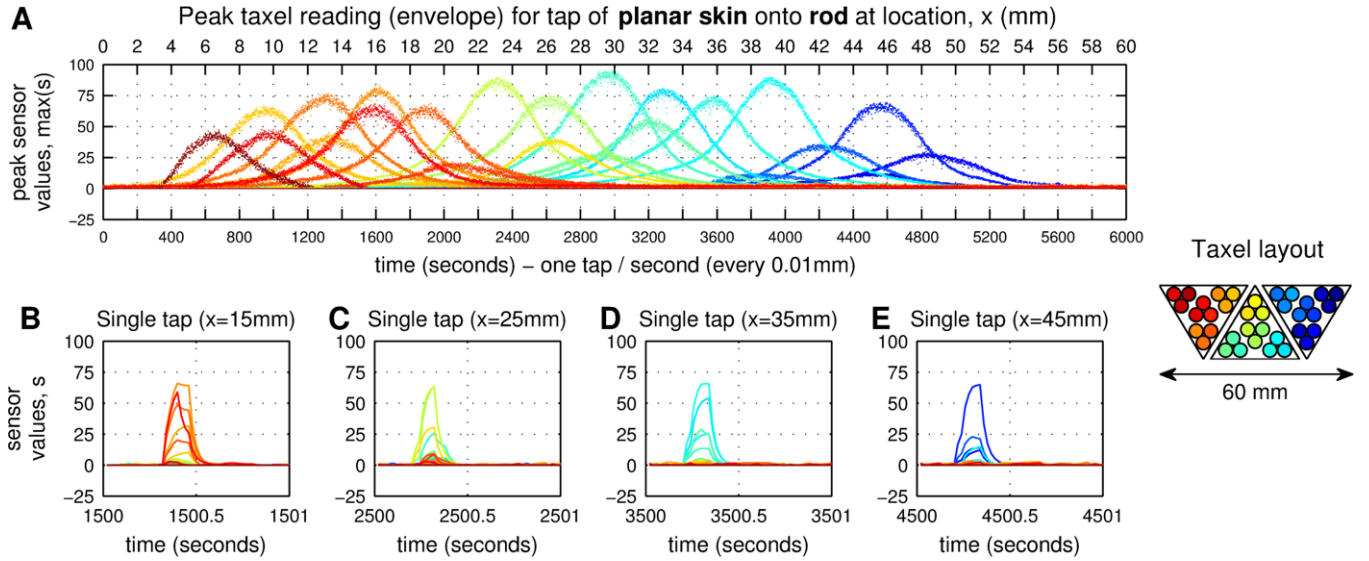


Fig. 12. Tactile data collected as some tactile skin taps against a test rod (dia. 6.4 mm) at constant rate of 1 tap/second, with 0.01 mm displacement after every tap to span a 50 mm range with 5000 taps. (B-E) Individual tap data taken from panel (A). Taxels are colored according to their layout on the skin. Sensor responses are collected at 8-bit resolution (maximum value 256); comparison with a pressure scale is given in ref. [27, Fig. 10].

across with centers spaced every 4 mm (Fig. 12A). Individual taps typically took  $\sim 0.1$  sec to reach peak amplitude, followed by rapid decay to baseline (Figs 12B-E). Notable differences between the skin and fingertip data are the larger number of taxels now traversed and their broader receptive fields.

The pattern of taxel pressures and their response amplitudes depend on the location of skin relative to the test rod (similarly to the fingertip and rod), permitting classification of where the rod is located relative to the skin.

2) *Passive Bayesian perception:* The perceptual acuity of the planar skin for locating the rod is assessed first with the same passive Bayesian method for robot perception that was applied to the fingertip and rod. Results are again generated with a Monte Carlo procedure (Sec. III-C), such that each contact tap *passively* remains at its initial location class.

Passive perceptual decisions of object location are evaluated for decision thresholds  $\theta_{\text{dec}}$  from 0-0.999, over  $N_{\text{loc}} = 60$  location classes spanning the 60 mm range across the skin (Fig. 13). Perception is generally of sub-taxel accuracy across this range, with localization errors  $e_{\text{loc}}(x) \lesssim 1$  mm (Fig. 13A), other than the extremities where the location error increases, as with the fingertip.

A typical localization accuracy for passive perception with the planar skin and rod is the mean localization error  $\bar{e}_{\text{loc}}$  over all possible sensing locations (Fig. 14A, red plot). This error  $\bar{e}_{\text{loc}} \sim 0.4$  mm is consistent with the 0-1 mm localization error  $e_{\text{loc}}(x)$  variability described above. In comparison with the rod

and fingertip (Sec. IV-A2), the location acuity is finer because the poor acuity at the extremities is limited to a smaller proportion of the overall range. That being said, we still expect that the perceptual performance can be improved by utilizing regions of relatively good acuity within the location range.

3) *Active Bayesian perception:* The acuity of the planar tactile skin locating a rod is now assessed with the same active method for robot perception that was applied to the fingertip and rod. Again we use a ‘fixation point’ policy, in which a best estimate of current location is used to calculate a relative move to a fixed location on the object. Like the fingertip, we take this fixation point at the center of the range ( $x_{\text{fix}} = 30$  mm) where the passive perception had good acuity. The range of decision thresholds  $\theta_{\text{dec}}=0-0.999$  remains unchanged from above, to permit comparison of the active and passive approaches.

As in previous sections, we measure perceptual performance by the mean localization error  $\bar{e}_{\text{loc}}$  over all initial contact locations (Fig. 14; green plots). The best accuracies were again for the higher decision thresholds (Fig. 14A) corresponding to decision times greater than 4-5 taps (Fig. 14C). Then active perception reaches an accuracy  $\bar{e}_{\text{loc}} \lesssim 0.18$  mm, finer than passive perception ( $\sim 0.4$  mm) and the (4 mm) taxel spacing (Table III).

Perceptual performance again depends on the number of location classes, considered over  $N_{\text{loc}} = 30-600$  with location class width  $60/N_{\text{loc}}$  mm, and the above-mentioned dependence on decision threshold (Figs 14A,B). The best perceptual errors

number of classes, $N_{\text{loc}}$	25	50	100	200	250	500
class width, $x_{\text{class}}$	2 mm	1 mm	0.5 mm	0.35 mm	0.2 mm	0.1 mm
mean decision error, $\bar{e}_{\text{loc}}$ (passive perception)	0.39 mm	0.44 mm	0.43 mm	0.40 mm	0.42 mm	0.41 mm
mean decision error, $\bar{e}_{\text{loc}}$ (active perception)	0.01 mm	0.04 mm	0.11 mm	0.12 mm	0.13 mm	0.18 mm
acuity, $\max(x_{\text{class}}, \bar{e}_{\text{loc}})$ (active perception)	2 mm	1 mm	0.5 mm	0.35 mm	0.20 mm	0.18 mm

TABLE III

ACTIVE PERCEPTUAL ACUITY DEPENDS ON LOCATION CLASS WIDTH. RESULTS ARE FOR MEAN DECISION TIMES OF 4 TAPS.

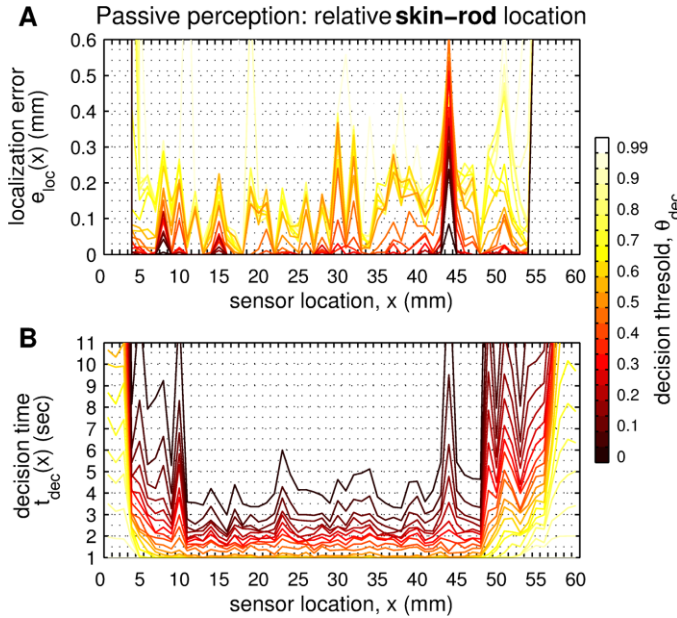


Fig. 13. Acuity of passive Bayesian perception depends on relative skin-rod location and decision threshold. (A) Localization error  $e_{loc}(x)$  and (B) decision time  $t_{dec}(x)$  plotted against sensor location  $x$ , with the color-scale denoting decision threshold (10000 trials per threshold, with  $N_{loc}=60$  location classes). Perceptual accuracy is best in the central location range.

increase with class number from  $\bar{e}_{loc} = 0.01$  mm (30 classes) to  $0.18$  mm (600 classes), while class resolution improves from 2 mm to 0.1 mm (Table III). Location accuracy and class resolution become similar between 300 and 600 classes, giving a best perceptual acuity of 0.18 mm.

Considering the taxel spacing is 4 mm for the planar skin, active perception gives a localization superresolution with twenty-fold improvement in acuity over sensor resolution.

## V. EXAMPLE APPLICATIONS

In this section, we describe two applications to illustrate how tactile superresolution can benefit robot task performance. Our expectation is that superresolution could offer far wider benefits for tactile robotics, but the following examples give a flavor of the benefits in a couple of different scenarios.

### A. Tactile object localization

Accurate tactile localization can benefit a wide range of robot tasks that involve placing an end effector precisely upon an object, from autonomous grasping and manipulation to autonomous devices for cutting, drilling and machining. Superresolution is directly relevant to these tasks because it enables task performance beyond the sensor resolution.

We now demonstrate that our methods for tactile superresolution apply not just to the rod stimuli considered in this paper, but also to more localized stimuli. The aim is to validate the method on an object contacting only a few taxels on the palm, rather than extended contact regions for rod stimuli, and also to clarify how the formalism applies to other stimuli.

The perceptual task is to determine the tangential (horizontal) location of a spherical test object (dia. 6.4 mm). We took a similar training and testing procedures as described earlier

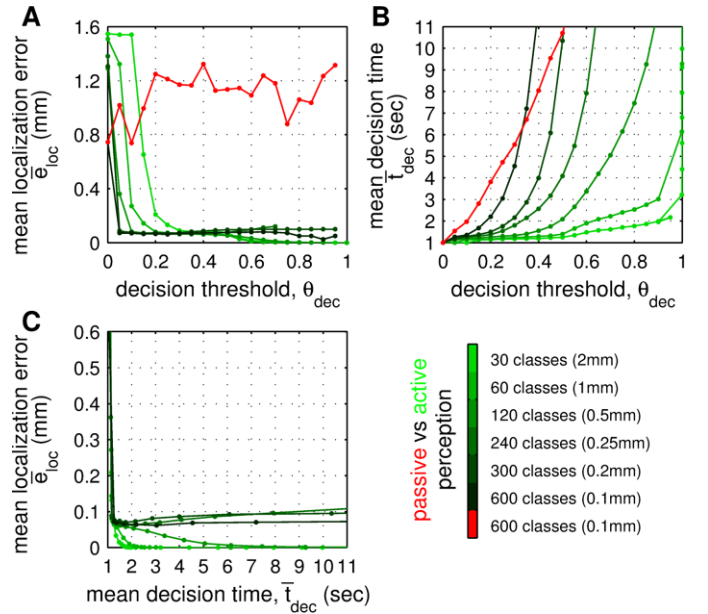


Fig. 14. Location-averaged performance for active and passive perception with the tactile skin. (A) Mean localization errors  $\bar{e}_{loc}$  and (B) decision times  $\bar{t}_{dec}$  plotted against decision threshold (10000 trials per threshold). Passive perception is shown in red and active perception in green. (C) Mean localization error against mean decision time. Active performs better than passive perception, and both improve with increasing decision threshold and decreasing class number.

in this paper (Sec. III), with a horizontal  $x$  range of 50 mm with taps every 0.01 mm (5000 taps), and the data collection repeated twice to give distinct training and test sets. We then repeated the analysis used for the rod stimulus in Sec. IV-B.

Passive perception of object location (Fig. 15) was more variable across the skin than found previously with the rod (*c.f.* Fig. 13; note change in scale), although the perceptual acuity remained typically below sensor resolution. We interpret this variability as from changes in the number and quality of the taxel contacts at different locations of the sphere on the skin; in contrast, the rod impinged over an extended region and was thus more likely to make good contacts with several taxels.

Active perception enabled the robot to avoid the issue of variable perception, by setting a fixation point at a good location for perception, which we chose at the 37 mm location class because of the broad minimum in Fig. 15. In consequence, high acuity perception of 0.1–0.2 mm mean location error can be attained (Fig. 16), of similar value to that for the rod stimulus on the fingertip and skin.

Therefore the active perception methods utilized here can attain superresolution in object localization that generalizes readily to various types of object. It is necessary to train the algorithms on the particular object to be localized. Once the methods are trained, they will attain superresolution in a manner suited for robustly placing an end effector precisely upon the object.

### B. Tactile contour following

Tactile contour following seeks to trace a tactile sensor around the edge of an object based on tactile information.

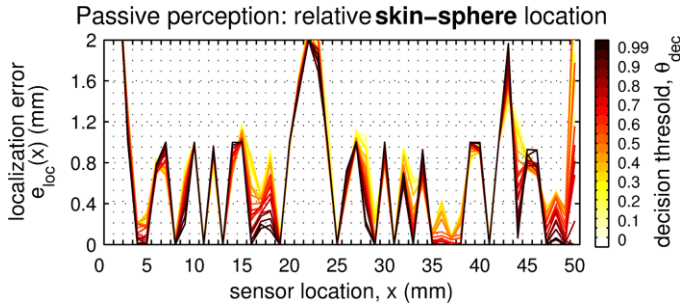


Fig. 15. Acuity of passive perception for the sphere and skin. Localization error  $e_{loc}(x)$  is plotted against sensor location  $x$ , with the color-scale denoting the decision threshold. Perceptual performance varies with location, with only some regions having consistently good performance (e.g. 35-38 mm).

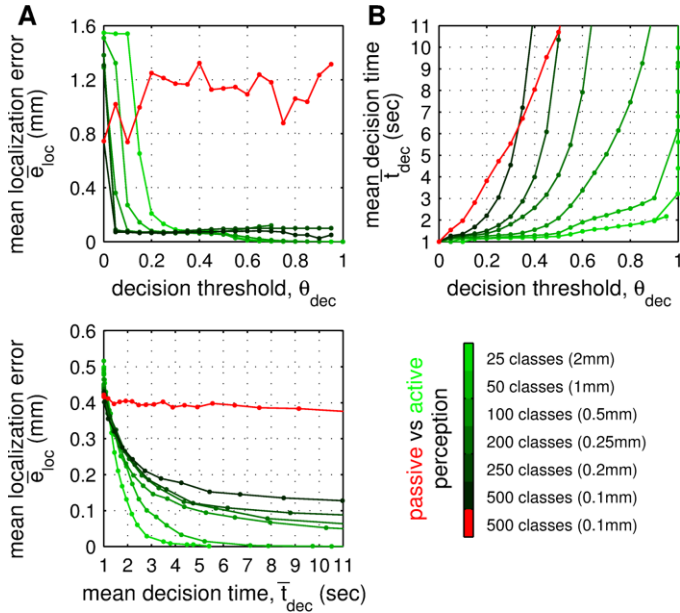


Fig. 16. Location-averaged performance for active and passive perception with the sphere and tactile skin. Mean localization error is plotted against mean decision time; the best acuity is around 0.1-0.2 mm after 4 contact taps.

Humans utilize contour following to perceive the shape of extended objects [36]. In robotics, the task is an example of a sensorimotor control strategy, of general interest in controlling robots via perceiving their surroundings. Autonomous contour following also has potential applications in surface quality control and inspection testing, in which a tactile sensor could be guided over areas of interest using tactile information.

A variant of the methods in this paper has been applied to tactile contour following, in which the tactile fingertip autonomously taps around the edge of an object [37]. The method perceives both the location and orientation of the edge relative to a tactile fingertip, and then uses this perceptual information to move the sensor a small distance along the edge of the object. Similar to the present study, the location and orientation are perceived over multiple taps, and an active perception strategy of moving the fingertip perpendicular to the edge employed to ensure the contact is good for perception.

Successful task performance was validated by having the fingertip tap around two circular objects and one irregular

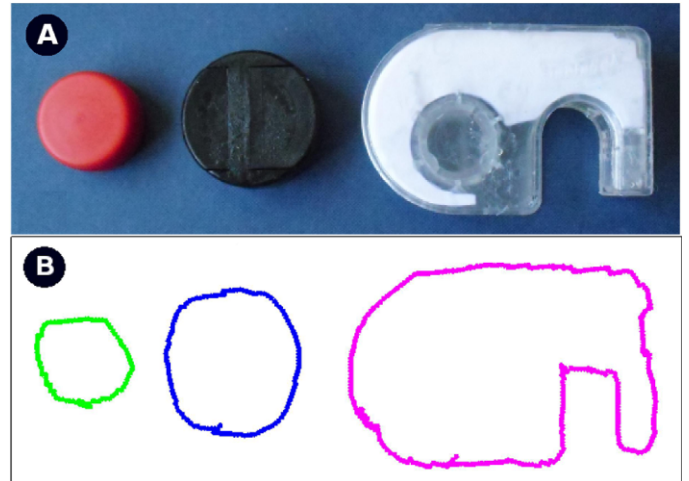


Fig. 17. Tactile hyperacuity applied to contour following. (A) Circles with 10 mm, 20 mm diameter and an asymmetric object used for validation. (B) Trajectories via active perception applied to sensorimotor control.

object (Fig. 17; ref. [37]). Since the fingertip was identical to that used in the other studies in this paper, the tactile sensor resolution was 4 mm. The traced contours were more accurate than this resolution, with mean error less than 1 mm. The superresolution was actually essential for task completion, since applying a passive method with poorer location acuity close to the sensor resolution caused the control to fail in tracing the objects [37]. The superresolution in the edge following task followed from the same reasons as those in the present study.

## VI. DISCUSSION

In this study, we demonstrated superresolution with a curved tactile fingertip and a planar region of tactile skin: for the fingertip localizing a rod, the best acuity was 0.12 mm, a thirty-five fold improvement over the (4 mm) sensor resolution; for the skin localizing a rod, the best acuity was 0.18 mm, better than twenty fold improvement over the sensor resolution. This hyperacuity is comparable with that of human vision and touch, which is typically 1-2 orders of magnitude better than the sensory receptor spacing [3], [7]. A combination of factors help attain this degree of superresolution, both in the construction of the tactile sensors and the methods for robot touch, which we now discuss.

### A. Construction of the tactile sensor

The construction of the tactile sensor is crucial for attaining superresolution. Both the tactile fingertip and planar tactile skin used here are variants of a taxel-based construction with the following key properties (see Figs 9,12): (i) the taxel receptive fields (areas sensitive to contact) are broader than the taxel spacing; (ii) the taxel contact sensitivity peaks in the center of the taxel and decreases gradually away from that peak; (iii) the taxels have good contact pressure resolution, as evident in the smooth change in contact sensitivity across the receptive field. The importance of these properties is that a contact against the tactile sensor will be encoded across

multiple taxels, with pressure readings that change smoothly and gradually with small changes in contact location. In consequence, location is represented within the contact data at a finer precision than the taxel spacing (sensor resolution), which appropriate computational methods can utilize to attain superresolution.

We are aware of other tactile sensors with similar response properties that may also have the potential for localization superresolution. Micro Electro Mechanical Systems (MEMS) based tactile sensors comprise arrays of taxel sensing elements, integrated with a layer of elastomeric skin-like material on the surface. One implementation as MEMS barometer chips covered in rubber (TakkStrip from TakkTile, MA, USA) has broad overlapping receptive fields with sensitivity to contact location that decreases from a central peak [38, Fig. 8]. Another MEMS-based sensor was explicitly bioinspired in its construction and application as a robotic finger, and similarly has overlapping receptive fields [39, Fig. 12]. Another biomimetic fingertip with soft tissue, bone and embedded sensors also has broad, overlapping receptive fields [40, Fig. 9].

The construction of several other taxel-based tactile sensors also seems appropriate for superresolution, in having discrete taxels covered with a soft ‘skin’ that transmits the contact across multiple taxels. Examples include the Biotac tactile fingertip from Syntouch, CA, USA [41] and the DLR artificial skin from the German Aerospace Center [42]. We expect that most tactile sensors based on a discrete taxel construction will attain superresolution, and in many cases this superresolution will be aided by a design in which a soft skin spreads the contact forces across multiple taxels, resulting in broad, overlapping receptive fields that vary smoothly with contact location.

For touch-based applications in future robotics, our expectation is that sensor optimization will be a sophisticated procedure, requiring modeling and empirical studies to customize the design to suit a robot’s intended use. Multiple design characteristics can impact on the sensor performance, including taxel density, spatial layout, pressure sensitivity and receptive field size or shape. These properties will depend non-trivially on the morphology of the sensor and its material construction. For example, a stiffer coating would distribute force over a larger area, giving broader but less sensitive receptive fields. We expect sensor optimization will be a complicated procedure (because of the large number of variables), although some recent developments in robot touch could ease this process. In particular, 3D-printed tactile sensors [43], [44] could accelerate the design-testing cycle for sensor customization, while finite element modeling of tactile sensors has the potential to enable a primarily simulation-based design process [45], [46].

### B. Computational method for perception

The tactile perception method is also key for attaining superresolution, because it must interpolate between multiple taxels to localize at a finer acuity than the taxel spacing. The Bayesian perception method used here implements the interpolation process by combining probability distributions

over distinct taxels, time within a single contact, and over multiple contacts. Thus, evidence from distinct taxels is fused to estimate contact location over many taxels and evidence from distinct tactile contacts is fused to further improve location acuity. Our method therefore has multiple aspects of geometrical superresolution [19], including both sub-taxel localization [20] from interpolating over taxel distributions, and multi-exposure noise reduction [21] by interpolating over measurements from distinct contacts.

Superresolution has also been achieved with geometric techniques not relying on Bayesian statistics. For example, digital image registration is a branch of computer vision that deals with geometric alignment of a set of images [47], and estimating that alignment can give tactile superresolution with a planar  $5 \times 5$  taxel array [23]. Image processing methods are continuing to be utilized in robot touch for planar sensors with large taxel arrays. Ho *et al* locate the position and orientation of objects using image moments over a  $44 \times 44$  taxel array [48], and we would expect such methods to achieve superresolution with suitable stimuli; indeed, related methods for tactile servoing with a  $16 \times 16$  array can reach sub-taxel resolution [49, Fig. 2]. However, such methods do not apply straightforwardly to the data used here because they rely on having flat arrays with a high density of tactile elements, whereas our tactile fingertip is curved and has only 12 taxels spaced 5 mm apart. Moreover, our data was taken over tapping contacts with temporal dynamics (*e.g.* Figs 9B-E), whereas imaging techniques rely on having a single image (or many versions of the same image). For these reasons and more, we found a Bayesian approach to provide a general yet simple and robust solution for implementing tactile perception with superresolution capability.

### C. Active perception

The final factor necessary for robust tactile hyperacuity is to use active control during perception. Our Bayesian perception method extends naturally to active perception by moving the sensor with a control strategy based on evidence received during the localization decision. Benefits of active Bayesian perception include: (i) an order-of magnitude improvement in acuity over passive methods [12]–[14]; (ii) robust perception in unstructured environments [12]; and (iii) relation to a general framework for simultaneous object localization and identification [13]. In consequence, a thirty-five fold improvement in perceptual acuity (from 4 mm to 0.12 mm) is obtained using an active control policy that centers the tactile fingertip on the rod, enabling robust superresolution.

To the best of our knowledge, the connection between active perception and superresolution (hyperacuity) has not been emphasized in the biology or engineering literatures. The main point is that perceptual acuity depends on how a sensor interacts with an object, which must thus be actively controlled to attain the best acuity. For example, in robot touch, the perceptual acuity is known to vary strongly with contact location [11]–[13], and thus passive perception performs badly when that contact location cannot be set *a priori*. This dependence between acuity and control is a general aspect

of biological and artificial perception [50], [51], from eye movements that perform visual tasks such as smooth pursuit, to actively controlling our fingers and hands for exploring and recognizing objects [52].

## VII. CONCLUSION

In this paper, we proposed that superresolution should be a central consideration for the design and application of artificial tactile sensors, just as hyperacuity is a fundamental aspect of biological perception. Tactile superresolution is aided by three key factors: *sensor construction*, to have multiple, overlapping, broad but sensitive receptive fields; *perceptual inference* that interpolates between these overlapping receptors to perceive at sub-taxel acuity; and *active perception*, to ensure robustness of the perception in unstructured environments. We envisage that these principles could become central to the construction and deployment of cheap yet high-acuity tactile sensors, which could be individually customized so that their design optimally matches their intended application in robot touch.

## REFERENCES

- [1] V. Marx, "Is super-resolution microscopy right for you?" *Nature Methods*, vol. 10, no. 12, pp. 1157–1163, 2013.
- [2] Editorial, "Method of the year 2008," *Nature Methods*, vol. 6, p. 1, 2009.
- [3] G. Westheimer, "Visual acuity and hyperacuity," *Handbook of Optics, Vol. III: Vision and Vision Optics*, pp. 4–1, 2009.
- [4] R. Dahiya, G. Metta, M. Valle, and G. Sandini, "Tactile sensing - from humans to humanoids," *Robotics, IEEE Transactions on*, vol. 26, no. 1, pp. 1–20, 2010.
- [5] N. Lepora, P. Verschure, and T. Prescott, "The state of the art in biomimetics," *Bioinspiration & biomimetics*, vol. 8, no. 1, p. 013001, 2013.
- [6] G. Westheimer, "Visual acuity and hyperacuity," *Investigative Ophthalmology*, vol. 14, no. 8, pp. 570–572, 1975.
- [7] J. Loomis, "An investigation of tactile hyperacuity," *Sensory Processes*, vol. 3, pp. 289–302, 1979.
- [8] A. Vallbo and R. Johansson, "The tactile sensory innervation of the glabrous skin of the human hand," *Active touch*, vol. 2954, 1978.
- [9] A. Schmitz, P. Maiolino, M. Maggiali, L. Natale, G. Cannata, and G. Metta, "Methods and technologies for the implementation of large-scale robot tactile sensors," *IEEE Trans Robotics*, vol. 27, no. 3, pp. 389–400, 2011.
- [10] G. Cannata, M. Maggiali, G. Metta, and G. Sandini, "An embedded artificial skin for humanoid robots," in *Multisensor Fusion and Integration for Intelligent Systems, 2008. MFI 2008. IEEE International Conference on*, 2008, pp. 434–438.
- [11] N. Lepora, U. Martinez-Hernandez, H. Barron-Gonzalez, M. Evans, G. Metta, and T. Prescott, "Embodied hyperacuity from bayesian perception: Shape and position discrimination with an icub fingertip sensor," in *Intelligent Robots and Systems (IROS), 2012 IEEE/RSJ International Conference on*, 2012, pp. 4638–4643.
- [12] N. Lepora, U. Martinez-Hernandez, and T. Prescott, "Active touch for robust perception under position uncertainty," in *Robotics and Automation (ICRA), 2013 IEEE International Conference on*, 2013, pp. 3005–3010.
- [13] ——, "Active bayesian perception for simultaneous object localization and identification," in *Robotics: Science and Systems*, 2013.
- [14] ——, "A SOLID case for active bayesian perception in robot touch," in *Biomimetic and Biohybrid Systems*, 2013, pp. 154–166.
- [15] R. Dahiya, P. Mittendorfer, M. Valle, G. Cheng, and V. Lumelsky, "Directions towards effective utilization of tactile skin-a review," 2013.
- [16] R. S. Dahiya and M. Valle, *Robotic Tactile Sensing*. Springer, 2013.
- [17] N. McWhirter, *The Guinness Book of World Records 1985*. Sterling Publishing Company, 1985, entry for "highest hyperacuity" (Dr D. Levi).
- [18] J. M. Loomis, "On the tangibility of letters and braille," *Perception & Psychophysics*, vol. 29, no. 1, pp. 37–46, 1981.
- [19] G. Westheimer, "Optical superresolution and visual hyperacuity," *Progress in Retinal and Eye Research*, vol. 31, no. 5, pp. 467–480, 2012.
- [20] Q. Tian and M. N. Huhns, "Algorithms for subpixel registration," *Computer Vision, Graphics, and Image Processing*, vol. 35, no. 2, pp. 220–233, 1986.
- [21] P. Debevec and J. Malik, "Recovering high dynamic range radiance maps from photographs," in *SIGGRAPH 97, Conference Proceedings*, 1997, pp. 369–378.
- [22] Z. Zalevsky and D. Mendlovic, *Optical superresolution*. Springer, 2004, vol. 91.
- [23] D. Van Den Heever, K. Schreve, and C. Scheffer, "Tactile sensing using force sensing resistors and a super-resolution algorithm," *Sensors Journal, IEEE*, vol. 9, no. 1, pp. 29–35, 2009.
- [24] M. Evans, C. Fox, M. Pearson, N. Lepora, and T. Prescott, "Whisker-object contact speed affects radial distance estimation," in *Robotics and Biomimetics (ROBIO)*, 2010, pp. 720–725.
- [25] M. Evans, C. Fox, N. Lepora, M. Pearson, J. Sullivan, and T. Prescott, "The effect of whisker movement on radial distance estimation: a case study in comparative robotics," *Frontiers in Neurorobotics*, vol. 6, 2012.
- [26] N. Lepora, U. Martinez-Hernandez, G. Pezzulo, and T. Prescott, "Active bayesian perception and reinforcement learning," in *Intelligent Robots and Systems (IROS), 2013 IEEE/RSJ International Conference on*, 2013, pp. 4735–4740.
- [27] A. Schmitz, M. Maggiali, L. Natale, and G. Metta, "Touch sensors for humanoid hands," in *IEEE International Symposium in Robot and Human Interactive Communication (RO-MAN)*, 2010, pp. 691–697.
- [28] J. Gold and M. Shadlen, "The neural basis of decision making," *Annu. Rev. Neurosci.*, vol. 30, pp. 535–574, 2007.
- [29] N. Lepora and K. Gurney, "The basal ganglia optimize decision making over general perceptual hypotheses," *Neural Computation*, no. 24, pp. 2924–2945, 2012.
- [30] A. Wald and J. Wolfowitz, "Optimum character of the sequential probability ratio test," *The Annals of Mathematical Statistics*, vol. 19, no. 3, pp. 326–339, 1948.
- [31] N. Lepora, C. Fox, M. Evans, M. Diamond, K. Gurney, and T. Prescott, "Optimal decision-making in mammals: insights from a robot study of rodent texture discrimination," *Journal of The Royal Society Interface*, vol. 9, no. 72, pp. 1517–1528, 2012.
- [32] N. Lepora, J. Sullivan, B. Hutchinson, M. Pearson, K. Gurney, and T. Prescott, "Brain-inspired bayesian perception for biomimetic robot touch," in *Robotics and Automation (ICRA), 2012 IEEE International Conference on*, 2012, pp. 5111–5116.
- [33] D. Ballard and A. Ozcanarli, "Eye fixation and early vision: Kinetic depth," in *Computer Vision., Second International Conference on*, 1988, pp. 524–531.
- [34] D. Ballard, "Animate vision," *Artificial intelligence*, vol. 48, no. 1, pp. 57–86, 1991.
- [35] N. Lepora, M. Evans, C. Fox, M. Diamond, K. Gurney, and T. Prescott, "Naive bayes texture classification applied to whisker data from a moving robot," *Neural Networks (IJCNN), The 2010 International Joint Conference on*, pp. 1–8, 2010.
- [36] S. Lederman and R. Klatzky, "Extracting object properties through haptic exploration," *Acta Psychologica*, vol. 84, no. 1, pp. 29–40, 1993.
- [37] U. Martinez-Hernandez, T. Dodd, L. Natale, G. Metta, T. Prescott, and N. Lepora, "Active contour following to explore object shape with robot touch," in *World Haptics Conference (WHC)*, 2013, pp. 341–346.
- [38] Y. Tenzer, L. Jentoft, and R. Howe, *Inexpensive and Easily Customized Tactile Array Sensors using MEMS Barometers Chips*, 2012.
- [39] H. Muhammad, C. Oddo, L. Beccai, C. Recchiuto, C. Anthony, M. Adams, M. Carrozza, D. Hukins, and M. Ward, "Development of a bioinspired MEMS based capacitive tactile sensor for a robotic finger," *Sensors and Actuators A: Physical*, vol. 165, no. 2, pp. 221–229, 2011.
- [40] K. Chathuranga, V. Ho, and S. Hirai, "A biomimetic fingertip that detects force and vibration modalities and its application to surface identification," in *Robotics and Biomimetics (ROBIO)*, 2012 IEEE International Conference on, 2012, pp. 575–581.
- [41] J. Fishel and G. Loeb, "Sensing tactile microvibrations with the biotact comparison with human sensitivity," in *Biomedical Robotics and Biomechatronics (BioRob), 2012 4th IEEE RAS & EMBS International Conference on*, 2012, pp. 1122–1127.
- [42] M. Strohmayer and D. Schneider, "The DLR artificial skin step II: Scalability as a prerequisite for whole-body covers," in *Intelligent Robots and Systems (IROS), 2013 IEEE/RSJ International Conference on*, 2013, pp. 4721–4728.
- [43] C. Chorley, C. Melhuish, T. Pipe, and J. Rossiter, "Development of a tactile sensor based on biologically inspired edge encoding," in *Advanced Robotics, 2009. ICAR 2009. International Conference on*, 2009, pp. 1–6.

- [44] B. Winstone, G. Griffiths, C. Melhuish, T. Pipe, and J. Rossiter, "TACTIP - tactile fingertip device, challenges in reduction of size to ready for robot hand integration," in *Robotics and Biomimetics (ROBIO), 2012 IEEE International Conference on*, 2012, pp. 160–166.
- [45] T. Le, P. Maiolino, F. Mastrogiovanni, A. Schmitz, and G. Cannata, "A toolbox for supporting the design of large-scale capacitive tactile systems," in *Humanoid Robots (Humanoids), 2011 11th IEEE-RAS International Conference on*. IEEE, 2011, pp. 153–158.
- [46] A.-V. Ho and S. Hirai, "Modeling and analysis of a frictional sliding soft fingertip, and experimental validations," *Advanced Robotics*, vol. 25, no. 3-4, pp. 291–311, 2011.
- [47] S. Zokai and G. Wolberg, "Image registration using log-polar mappings for recovery of large-scale similarity and projective transformations," *Image Processing, IEEE Transactions on*, vol. 14, no. 10, pp. 1422–1434, 2005.
- [48] A.-V. Ho, T. Nagatani, A. Noda, and S. Hirai, "What can be inferred from a tactile arrayed sensor in autonomous in-hand manipulation?" in *Automation Science and Engineering (CASE), 2012 IEEE International Conference on*, 2012, pp. 461–468.
- [49] Q. Li, C. Schürmann, R. Haschke, and H. Ritter, "A control framework for tactile servoing," in *Robotics: Science and Systems*, 2013.
- [50] R. Bajcsy, "Active perception," *Proceedings of the IEEE*, vol. 76, no. 8, pp. 966–1005, 1988.
- [51] N. Lepora, "Active tactile perception," *Scholarpedia*, vol. 10, no. 3, p. 32364, 2015.
- [52] S. Lederman and R. Klatzky, "Hand movements: A window into haptic object recognition," *Cognitive psychology*, vol. 19, pp. 342–368, 1987.



**Nathan F. Lepora** received the B.A. degree in Mathematics and the Ph.D. degree in Theoretical Physics from the University of Cambridge, U.K.

He is currently a Lecturer and Program Director for the Robotics MSc with the Department of Engineering Mathematics, University of Bristol (UOB), U.K., and is affiliated with the Bristol Robotics Laboratory, UOB and UWE, U.K. He is also a honorary research fellow at the Sheffield Center for Robotics, University of Sheffield, U.K., where he was a Research Associate then Fellow from 2005–2013. He has been program chair for the International Conference 'Living Machines' in 2012 and 2013. His research interests span robotics and neuroscience, focussing on robot and animal perception, artificial and natural decision making, and biomimetics.



**Uriel Martinez-Hernandez** received the B.Sc. degree in Communications and Electronics from the Instituto Politecnico Nacional, Mexico City, Mexico in 2005 and the M.Sc. degree in Computer Sciences from the Centro de Investigacion y de Estudios Avanzados del Instituto Politecnico Nacional, Mexico City, Mexico in 2008.

He has a Ph.D. degree in Automatic Control and Systems Engineering from the University of Sheffield, Sheffield, U.K., and is currently a Research Associate at the Department of Psychology

and the Sheffield Centre for Robotics (SCentRo) at the University of Sheffield, Sheffield, UK. His research interests include robot perception and control.



include computational

**Mathew Evans** received the BSc degree in Psychology, the MSc degree in Computational and Systems Neuroscience, and the PhD degree from the Department of Psychology, University of Sheffield, UK, in 2013.

He was previously a Research Associate at the Department of Psychology and the Sheffield Centre for Robotics (SCentRo) at the University of Sheffield, Sheffield, UK. He is currently a Research Associate at the Department of Psychology at the University of Manchester, Manchester, UK. His research interests methods for active touch sensing and robotics.



**Lorenzo Natale** received the Electronic Engineering degree (with honors) and the Ph.D. degree in robotics from the University of Genoa, Italy, in 2000 and 2004.

He was with the Laboratory for Integrated Advanced Robotics, University of Genoa. Between 2005 and 2006, he was a Postdoctoral Researcher with the Humanoid Robotics Group, Computer Science and Artificial Intelligence Laboratory, Massachusetts Institute of Technology, Cambridge. He is currently a Team Leader with the Italian Institute of Technology, Genova. His current research interests include developmental robotics, sensorimotor learning, and perception in artificial and biological systems, as well as software development and integration in robotics.



**Giorgio Metta** received the M.S. degree (Hons.) in 1994 and the Ph.D. degree in 2000, both in electronic engineering, from the University of Genoa, Italy.

From 2001 to 2002, he was a Postdoctoral Associate with the Artificial Intelligence Laboratory, Massachusetts Institute of Technology, Cambridge. He has been an Assistant Professor with the Dipartimento di Informatica Sistemistica e Telematica, University of Genoa, since 2005. Since 2006, he has also been a Senior Scientist with the Robotics, Brain, and Cognitive Sciences Department, Italian Institute of Technology, Genoa. His current research interests include biologically motivated humanoid robotics and, in particular, the development of artificial systems that show some of the abilities of natural systems. He is the author of more than 100 publications, and also engaged as a Principal Investigator and Research Scientist in several international and national funded projects.



**Tony J. Prescott** received the M.A. degree in psychology from University of Edinburgh, Edinburgh, U.K., the M.Sc. degree in Artificial Intelligence from the University of Aberdeen, Aberdeen, U.K., and the Ph.D. degree from the Department of Psychology, University of Sheffield, Sheffield, U.K., in 1994.

He is currently a Professor of cognitive neuroscience with the Department of Psychology, University of Sheffield. He is also a Permanent Research Fellow with the Bristol Robotics Laboratory, Bristol, U.K. He has authored more than 60 publications in psychology, neuroscience, computational modeling and robotics. His research interests include the biological and brain sciences, particularly concerned with understanding the evolution, development, and function of natural intelligence and the investigation of computational neuroscience models of animal and human intelligence and in testing these models in biomimetic robots.